QUARTERLY JOURNAL OF THE ROYAL METEOROLOGICAL SOCIETY
Q. J. R. Meteorol. Soc. **134**: 1253–1268 (2008)
Published online 9 July 2008 in Wiley InterScience
(www.interscience.wiley.com) DOI: 10.1002/qj.281

Dependence of vortex axisymmetrization on the characteristics of the asymmetry

Jiayi Peng,[a]*Melinda S. Peng[b†] and Tim Li[c]
[a] *International Pacific Research Center, University of Hawaii at Manoa, Honolulu, USA*
[b] *Naval Research Laboratory, Monterey, California, USA*
[c] *School of Ocean and Earth Science and Technology, University of Hawaii at Manoa, Honolulu, USA*

ABSTRACT: This study investigates how different characteristics of initial asymmetries, including their positions and profiles, can impact on the vortex axisymmetrization process for barotropic vortices. When an initial disturbance is placed near the core of a vortex, a new asymmetry is generated inside the original asymmetry and grows due to its upshear tilt. Differential basic-state rotation then shifts the phase to a downshear tilt and the asymmetry weakens. As the initial radius of the imposed asymmetry is increased, the initial upshear tilt of the asymmetry decreases. There is also a decrease in the efficiency with which the differential rotation shifts the phase tilt from upshear to downshear. The latter is related to differential radial propagation of the asymmetry in the form of vortex Rossby waves. These two mechanisms that are position-dependent act against each other. There is an optimal radius at which the energy exchange between the symmetric and asymmetric flows is maximized. For a range of very different basic-state profiles examined here, the optimal radius is around 1.5 to 2 times the radius of the maximum wind. The initial growth of asymmetries with higher azimuthal wavenumbers is weaker than their lower-wavenumber counterparts due to a smaller upshear phase tilt with their smaller azimuthal length-scales.

Nonlinearity reduces the magnitude and multiple perturbations of the newly induced inner asymmetry, and also limits the radial propagation of the asymmetry. The further the asymmetry is away from the core, the slower the axisymmetrization is. Depending on the position of the initial asymmetry, the basic state can have an increase of the maximum wind, a double-peak profile, or an increase of its outer wind profile through axisymmetrization.

KEY WORDS optimal radius; barotropic vortices

Received 6 December 2007; Revised 14 May 2008; Accepted 27 May 2008

1. Introduction

Due to the rapid rotation of fluid around a hurricane-like vortex near the core, asymmetric disturbances generated by external forcing such as convection will tilt in the direction of the basic-state shear so that energy is being transferred from the asymmetries to the symmetric part through eddy momentum flux. This process, called axisymmetrization, has been suggested as a mechanism during the formation and intensity change of tropical cyclones. Some previous studies on the axisymmetrization are reviewed briefly here.

Melander *et al*. (1987) and McCalpin (1987) are among the early studies identifying the axisymmetrization process in geophysical fluid dynamics. Sutyrin (1989) suggested that the axisymmetrization occurs as a result of differential rotation of the fluid and is similar to disturbance decay in rectilinear flow with simple shear (Case, 1960). Carr and Williams (1989) considered the small-amplitude disturbance axisymmetrized by a steady Rankine vortex. Their results indicated that the damping rate of perturbations is proportional to the square of the azimuthal wavenumber.

Vortex Rossby waves, originally proposed by MacDonald (1968), bear many similarities with the planetary Rossby waves, as the radial gradient of vorticity in a vortex is dynamically equivalent to the planetary vorticity gradient of the Earth system. The work by Guinn and Schubert (1993) indicated that hurricane spiral bands can be formed by the breaking of potential vorticity (PV) waves when the core of a symmetric vortex is perturbed or by the merging of a vortex with higher-order potential vorticity disturbances. Smith and Montgomery (1995) examined the dependence of axisymmetrization on the azimuthal wavenumber and the asymmetric radial structure in a barotropic model. A truly inviscid mechanism that favours the decay of high-wavenumber perturbations over that of low wavenumbers was identified. In an attempt to understand spiral bands in tropical cyclones, Montgomery and Kallenbach (1997, hereafter

* Correspondence to: Jiayi Peng, International Pacific Research Center, University of Hawaii at Manoa, 1680 East West Road, Honolulu, HI 96822, USA. E-mail: Pengj@hawaii.edu
† The contribution of Melinda S. Peng to this article was prepared as part of her official duties as a United States Federal Government Employee.

MK97) described the axisymmetrization process through the propagation of vortex Rossby waves in a sheared vortex. A dispersion relation for the vortex Rossby waves, analogous to the one for the planetary Rossby waves, was obtained. In the sheared basic flow, the radial wavenumber is changing with time and radial distance due to a non-constant vorticity gradient. MK97 related the propagation of these waves to intensity changes in hurricane-like vortices.

Möller and Montgomery (1999, hereafter MM99) used a nonlinear asymmetric balance model to investigate the evolution of asymmetries with different radial wavenumbers in a hurricane-like vortex. The asymmetries propagate both inward and outward in the early stage and eventually all outward. Their kinematics and wave-mean flow interactions are characterized by mechanisms associated with the vortex Rossby waves (MK97). In the context of a three-dimensional balance model, Möller and Montgomery (2000) investigated the structure and intensity evolution of a tropical cyclone, and showed that vortex Rossby waves propagated both radially and vertically.

These studies as well as other related studies (Montgomery and Enagorio, 1998; Nolan and Farrell, 1999a,b; Shapiro, 2000; Enagorio and Montgomery, 2001) indicate that asymmetric vorticity perturbations introduced into the vicinity of a stable hurricane-like vortex lead to the intensification of the vortex. Most of these studies are based on a two-dimensional framework and considered momentum asymmetries as the end result of convective heating. Nolan and Montgomery (2002) and Nolan and Grasso (2003), in their two-part study, took one step closer to reality by considering asymmetric temperature perturbations in a three-dimensional framework. In part I it was shown that the thermal asymmetries first went through a rapid adjustment to hydrostatic balance with concomitant gravity wave radiation and the remaining vorticity perturbations went through axisymmetrization. In part II it was found that the response of the symmetric vortex to the evolving asymmetries has a negative effect on the overall intensity. This contrasts with earlier studies, such as those cited here. The changes caused by the asymmetries to the symmetric vortex were also very small. Möller and Shapiro (2005) showed that a diabatic-heating-induced asymmetry that was imposed on a hurricane-like vortex had a long-term effect on the vortex with episodes of weakening and strengthening.

In this study, we revisit the axisymmetrization process caused by imposing asymmetries of different initial positions and structures in a barotropic framework. Linear simulations are investigated first for better understanding, followed by nonlinear simulations. The initial asymmetry is prescribed as a vorticity perturbation. In Nolan and Grasso (2003), a thermal forcing induced very large pressure fluctuations in the early stage compared with a velocity forcing, but the final near-steady states were comparable for both forcings.

The outline of this paper is as follows. A brief description of the experimental design is given in Section 2. Results from the linear and nonlinear simulations are discussed in Sections 3 and 4, respectively. The summary and conclusion are given in Section 5.

2. Model description

2.1. The model

While one can use the vorticity equation for a barotropic study, we formulate the numerical models so that they can be used for baroclinic studies in the future. The models (see the appendix) sit on a constant-f plane with the Coriolis parameter $f = 5 \times 10^{-5}$ s^{-1} and the characteristic value for time $T = 1/f = 2 \times 10^4$ s. A non-dimensional time $t = 0.18$ corresponds to 1 hour. The characteristic values for the velocity and horizontal length-scales are $C = 50$ m s^{-1} and $L = CT = 1000$ km, and the Rossby number equals 1 for our vortex.

The numerical scheme is the fourth-order Runge–Kutta scheme with an increment of 0.002 (40 s). The Matsuno scheme (Shen *et al.*, 2003) is applied to calculate the advection terms, and the second-order centred difference is used for the approximation of space derivatives. A second-order diffusion is applied every 0.18 in time, with the non-dimensional coefficient equal to 1.4×10^{-6} to ensure numerical stability. The model covers a 2×2 (2000 km $\times$ 2000 km) area with a grid resolution of 0.002 (2 km) in both x and y directions. The lateral boundary condition is radiative. All the simulations are carried out to time 4.32 (24 hours). Most of the results shown are up to time 2.16 (12 hours), during which the major axisymmetrization process occurs.

2.2. Experiment design

The tangential wind of basic-state hurricane-like profile is defined as

$$V(r/R_{\max}) = V_{\max}\frac{2(r/R_{\max})}{1+(r/R_{\max})^2}, \tag{2.1}$$

where the maximum tangential wind $V_{\max} = 0.5$ (25 m s^{-1}), and the radius of maximum wind (RMW) $R_{\max} = 0.1$ (100 km). Note that while the tangential wind shear changes sign at RMW (Figure 1(a)), the angular velocity (V/r) deceases monotonically with radius (Figure 1(b)). It is more convenient to explain the vorticity or kinetic energy change in terms of angular velocity instead of the tangential wind in cylindrical coordinates (given later). The vorticity maximum is located at the centre of the vortex (Figure 1(c)), decreasing with radius, and the maximum vorticity gradient is situated at $r = 0.044$ (Figure 1(d)).

If the initial vorticity asymmetry has a wavenumber-one structure in the azimuthal direction, the flow associated with the asymmetry will advect the vortex centre and, as a consequence, a fast-growing mode will develop near the vortex core region. This artifact does not represent the growth of a normal mode and is therefore called a 'pseudomode' (MK97). To avoid the complication

DOI: 10.1002/qj

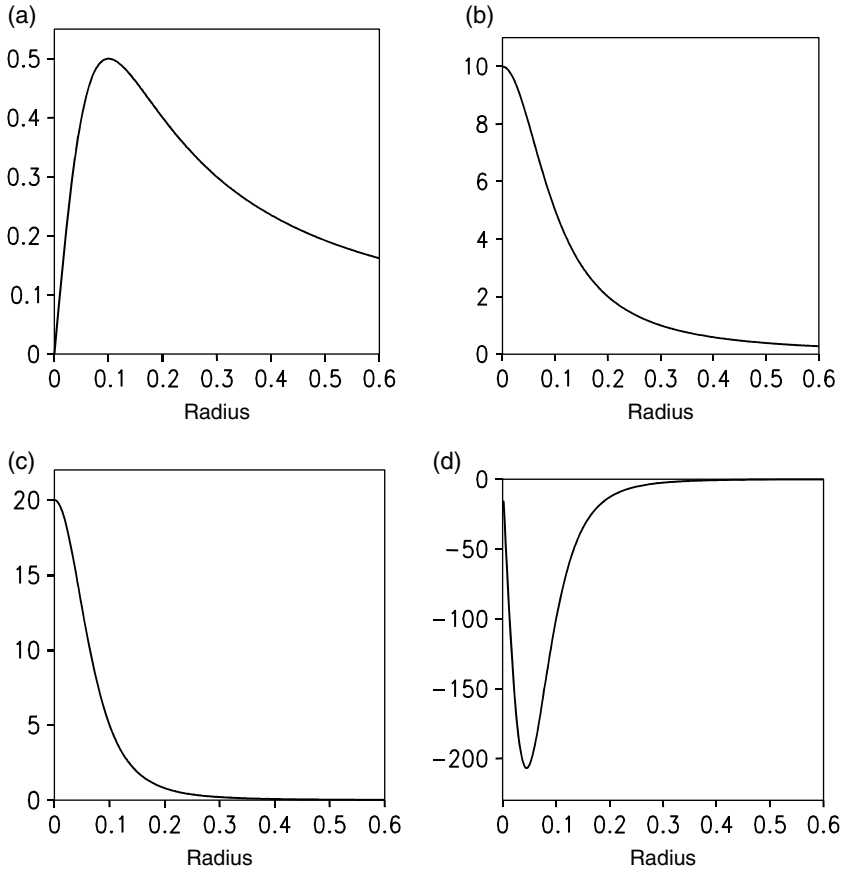

Figure 1. Radial profiles of the symmetric, hurricane-like vortex in non-dimensional form: (a) tangential wind (unit 50 m s^{-1}), (b) angular velocity (unit 5×10^{-5} s^{-1}), (c) vorticity (unit 5×10^{-5} s^{-1}) and (d) vorticity gradient (unit 5×10^{-11} m^{-1} s^{-1}). The unit of radius is 1000 km.

associated with the pseudomode, our initial asymmetry has either a wavenumber-two or -three structure in the azimuthal direction. The initial asymmetry is prescribed by a vorticity perturbation:

$$\zeta' = 5 \exp\left\{-\frac{1}{2}\left(\frac{r - R_p}{\sigma}\right)^2\right\} \cos(k\lambda), \qquad (2.2)$$

where r is the radial distance, λ the azimuthal angle, and k the azimuthal wavenumber. The radial parameter R_p controls the position of the initial asymmetry and σ determines the radial scale (or size) of the asymmetry. Our experiments include two radial scales, one with $\sigma = 0.025$ (a wide profile) and one with $\sigma = 0.0125$ (a narrow profile) and they are placed at different locations (Figure 2).

To investigate how the initial position of an asymmetry affects the axisymmetrization processes, three sets of experiments are carried out first with the wide radial profile and a wavenumber-two structure. The first set of experiment has its maximum initial perturbation placed at the RMW ($R_p = 0.1$), denoted as case LT010 for the linear case and NT010 for the nonlinear case (Figure 2, solid line). The second set has $R_p = 0.2$, denoted as LT020 and NT020, and $R_p = 0.3$ in the third set, denoted as LT030 and NT030 (Figure 2, long-dashed line). More cases, with different initial positions of the asymmetries, are

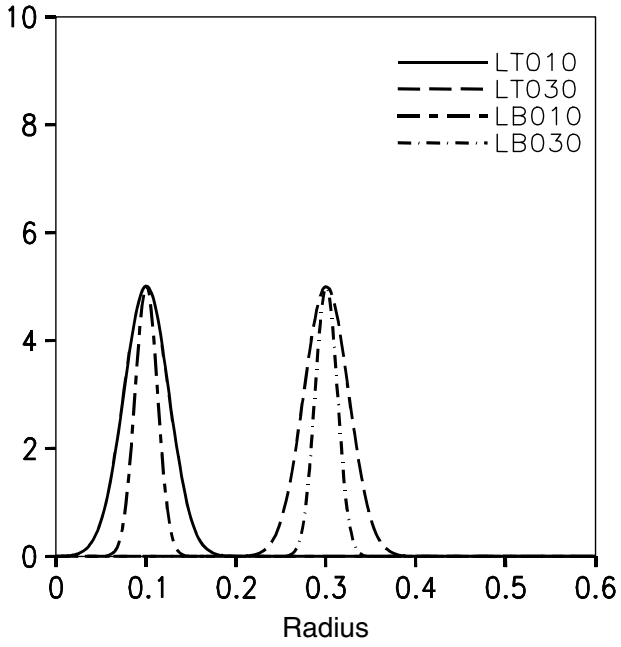

Figure 2. Radial profiles of the initial non-dimensional asymmetric vorticity amplitudes with the maximum located at two different positions: radius of 0.1 (for experiments LT010, LB010), and 0.3 (for experiments LT030, LB030) with the wide (solid and long dash) or the narrow (long-short dash and dot-dash) initial perturbations. The unit of radius is 1000 km.

DOI: 10.1002/qj

also carried out and will be explained later. Experiments with a wavenumber-three initial asymmetry are identified as LU010, LU020, etc., for linear cases with different initial positions. Asymmetries with a narrower profile are denoted as LB010, LB020, etc. No wavenumber-three cases are studied for the narrow profile. The description of the experiments is given in Table I.

Note that, since the initial perturbations are prescribed by the vorticity, asymmetries at different locations with the same vorticity would have different wind speed and kinetic energy (KE). The greater the distance from the centre, the larger the KE is for the same vorticity maximum. This effect will be investigated and discussed later.

All the model outputs are interpolated to a cylindrical coordinate system centred at the vortex centre and each variable is decomposed into a symmetric part and an asymmetric component, e.g. $u = \overline{u} + u'$, $v = \overline{v} + v'$. From this point on, a variable with a bar notation represents the symmetric part and a prime denotes the departure from the symmetry.

3. Linear axisymmetrization

3.1. Initial asymmetries with the broad profile and a wavenumber-two structure

The first linear case (LT010) considers an initial wavenumber-two vorticity asymmetry at the RMW with the broad profile (Figure 2, solid line). The temporal evolution of the vorticity and the corresponding KE in the radial direction is displayed in Figure 3(a, d). Immediately after the initial time, a weak asymmetry is induced where the absolute value of the basic vorticity gradient is largest. This new inner asymmetry grows until 0.54 and weakens afterwards (Figure 3(a, d)). Both the newly generated inner disturbance and the original asymmetry move outward while decaying. The general evolution of the vorticity field is very similar to the results of MK97.

The corresponding asymmetric kinetic energy (Figure 3(d)) shows a less pronounced signal of the inner asymmetry than the vorticity field (Figure 3(a)) due to a larger contribution from the curvature term to the vorticity as the radial distance gets smaller.

To understand the evolution of the asymmetric perturbation more clearly, the linear vorticity equation in a cylindrical coordinate is examined.

$$\frac{\partial \zeta'}{\partial t} = -\frac{\overline{v}}{r}\frac{\partial \zeta'}{\partial \lambda} - u'\frac{\partial \overline{\zeta}}{\partial r}, \tag{3.1}$$

where u' is the asymmetric radial wind, $\overline{v}$ the symmetric tangential wind, ζ' the asymmetric vorticity, and $\overline{\zeta}$ the symmetric vorticity. Note that the angular velocity appears in the first term of the right-hand side of (3.1).

Figure 4 shows the evolution of the asymmetric vorticity, the two terms on the right-hand side of (3.1), and the sum of them for the LT010 case. These fields are plotted in the radial and azimuthal coordinates for better viewing of the phase tilt. An increasing azimuthal (tangential) angle is downstream for the basic-state cyclonic flow. A phase line parallel to the y-axis has no phase tilt with respect to the basic-state angular velocity (Figure 1(b)), while a phase line with an increasing (decreasing) tangential angle outward is tilting upshear (downshear). The maximum positive vorticity advection by the symmetric wind is downstream from the maximum asymmetric vorticity (Figure 4(a)) while the vorticity change by the asymmetric radial wind induces maximum (positive) vorticity tendency upstream (Figure 4(b)). The combined effect of these two terms leads to a two-way tilted asymmetric vorticity at time 0.18 (Figure 4(d)). The phase tilt of the total asymmetry, defined by the line connecting the centres of the new inner asymmetry and the original

Table I. Parameters of initial perturbations for each experiment.

Case name ($\sigma = 0.025$, k = 2)	Position	Case name ($\sigma = 0.025$, k = 3)	Position	Case name ($\sigma = 0.0125$, k = 2)	Position
LT010 (NT010)	0.10	LU010	0.10	LB005	0.05
LT011	0.11	LU012	0.12	LB006	0.06
LT012	0.12	LU014	0.14	LB007	0.07
LT013	0.13	LU015	0.15	LB008	0.08
LT014	0.14	LU016	0.16	LB009	0.09
LT015 (NT015)	0.15	LU018	0.18	LB010	0.10
LT016	0.16	LU020	0.20	LB012	0.12
LT017	0.17	LU022	0.22	LB014	0.14
LT018	0.18	LU024	0.24	LB016	0.16
LT019	0.19	LU025	0.25	LB018	0.18
LT020 (NT020)	0.20	LU026	0.26	LB020	0.20
LT022	0.22	LU028	0.28	LB022	0.22
LT024	0.24	LU030	0.30	LB024	0.24
LT025 (NT025)	0.25			LB026	0.26
LT026	0.26			LB028	0.28
LT028	0.28			LB030	0.30
LT030 (NT030)	0.30				

DOI: 10.1002/qj

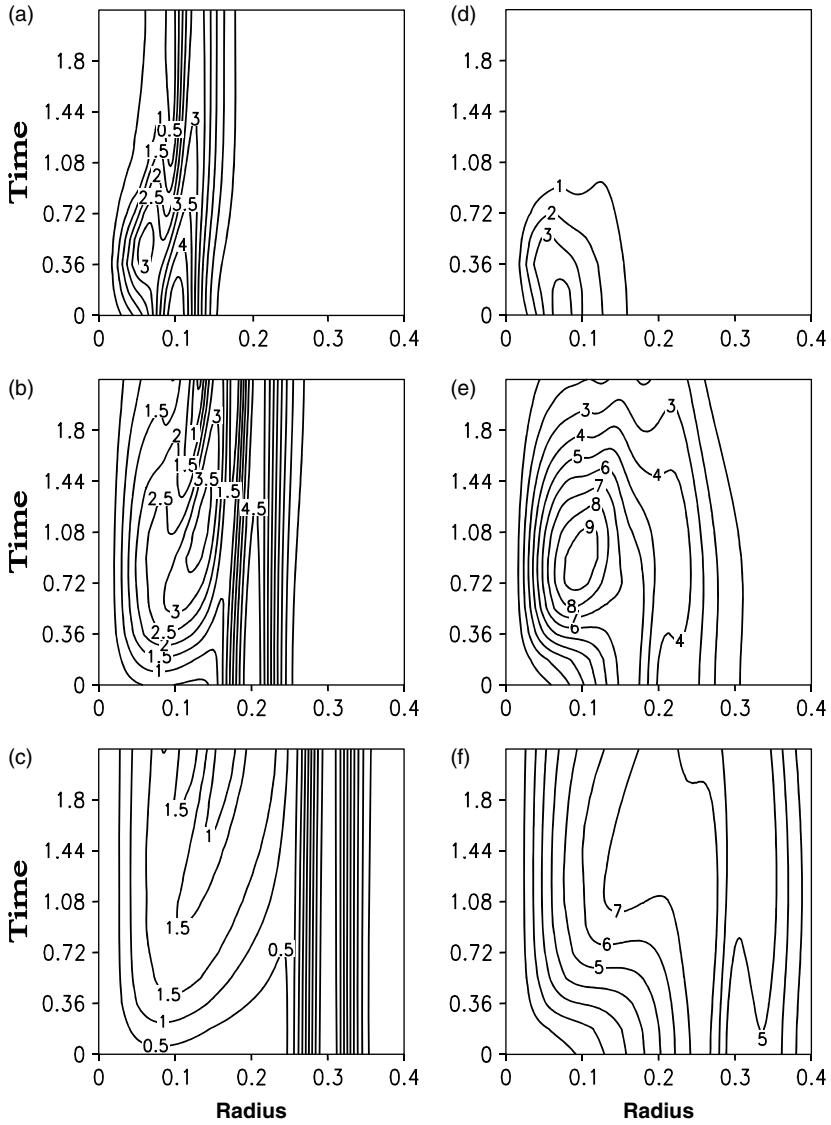

Figure 3. The time–radius cross-section of (a–c) the asymmetric vorticity amplitude for wavenumber two and (d–f) kinetic energy in the linear case (a, d) LT010, (b, e) LT020 and (c, f) LT030 for the initial asymmetry with a wide radial profile and tangential wavenumber-two perturbations. The unit of radius is 1000 km, and the unit of time 0.18 = 1 hour.

asymmetry, is upshear which allows the asymmetry to grow in the early stage (Figure 3(a, d)). Due to differential rotation, the phase turns to neutral by time 0.54 and the inner asymmetry reaches its maximum intensity (Figure 4(e)). Beyond this time, the asymmetry acquires a downshear tilt and weakens. Later, the asymmetry is significantly sheared and wraps round the centre while migrating outward gradually (Figure 4(f)).

In case LT020 where the initial asymmetry is located at twice the RMW, a much larger asymmetry is generated inside the initial asymmetry and it propagates outward gradually (Figure 3(b, e)). The local change of the vorticity from (3.1) is shown in Figure 5. The maximum of the first term on the right-hand side of (3.1) follows the position of the initial asymmetry to an outer radius while the second term remains close to that in the LT010 case (slightly outward) as it is dominated by the radial gradient of the basic state vorticity (figures not shown). The sum of these two terms shows two widely separated centres in the radial direction with opposite signs (Figure 5(a)). The phase tilt of the asymmetry is upshear in the early stage as in the LT010 but the phase angle is smaller. However, the effect of the differential rotation is also smaller in LT020 as the asymmetry is located further outward, allowing the upshear tilt to sustain longer until time 1.08 (Figure 5(c)) versus 0.54 in LT010 (Figure 4(e)). The same process repeats itself to induce additional inner asymmetries by the newly generated asymmetry (Figure 5(c, d)). These additional asymmetries are much weaker and play small roles in the axisymmetrization process. While the new asymmetries propagate outward, the initial asymmetry shows little outward propagation (Figures 3(b) and 5) as they are located where the basic-state vorticity gradient is very small (MK97). This is significant in vortex axisymmetrization as it determines where the asymmetry will deposit energy on the symmetric component that will be revealed in the nonlinear simulation later.

DOI: 10.1002/qj

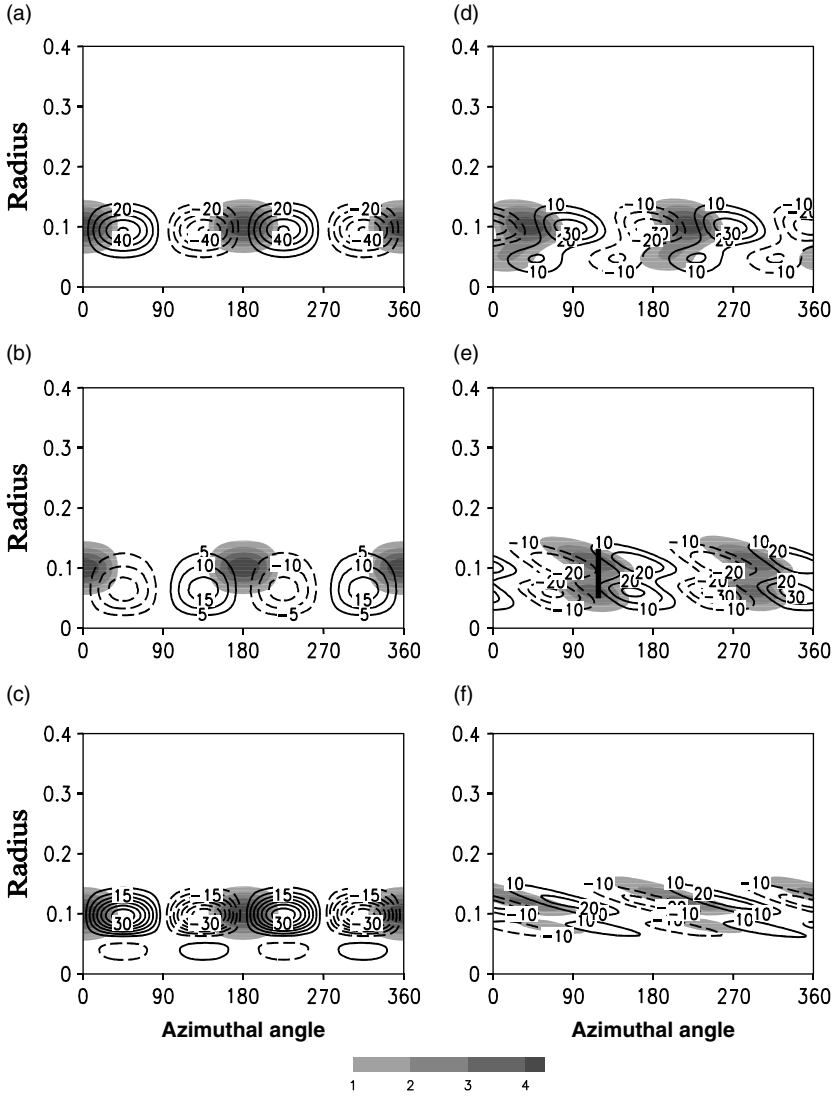

Figure 4. The vorticity advection at time 0.0 (unit 2.5×10^{-9} s^{-2}) by (a) the mean flow, (b) the perturbation flow, and the total vorticity tendency at time (c) 0.0, (d) 0.18, (e) 0.54 and (f) 1.08 for LT010. Shading represents the positive asymmetric vorticity (unit 5×10^{-5} s^{-1}). An increasing azimuthal angle is downstream for the basic cyclonic flows. The basic angular velocity decreases with the radius (Figure 1(b)) and the solid line in (e) indicates the phase line of the asymmetry.

The overall pattern of the asymmetric vorticity change (Figure 6) in LT030 (initial asymmetry located at $3R_{\max}$) is very similar to the LT020 case, except that the magnitudes are weaker. The first term on the right-hand side of (3.1) follows the initial asymmetry to an even greater radius while the second term is located roughly at the same place. The combination of the two is a two-cell vorticity change that is out of phase with a large separation between them (Figure 6(a)). The phase tilt of the asymmetry shown in Figure 6(b) is even smaller than in LT020 for the same time (Fig 5(b)). However, it also takes longer for the phase line to start tilting downshear (Figure 6(c) at time 1.62 versus Figure 5(c) at time 1.08). Contrary to the first two cases, there is little wrap-around of the disturbances even at a late stage due to much smaller shear of the basic vortex in the outer radius.

The time evolution of the asymmetric vorticity and the KE (Figure 3(c, f)) is similar to the LT020 case. The difference is that the asymmetric vorticity and KE for the new inner asymmetry is much weaker and it reaches its maximum slower than in the LT020 case.

As observed from our cases, new asymmetries are induced inward of the original asymmetry. Initially, the phase tilt of the asymmetry is upshear and the asymmetry extracts energy from the basic state. The upshear tilt is then reversed by the basic-state flow and the asymmetry weakens. The impact of this process on the basic state which will be shown in the nonlinear simulation depends on the early-stage phase angle and how long will this phase tilt remain upshear. The relative phase tilts among these three cases are shown in Figure 7. Figure 7(a–c) contains the asymmetric vorticity and the phase lines at time 0.18 for LT010, LT020 and LT030. The three phase lines are grouped on the right of Figure 7(d). The corresponding phase lines at time 0.54 are shown on the left of Figure 7(d). It is clear that, the further out

DOI: 10.1002/qj

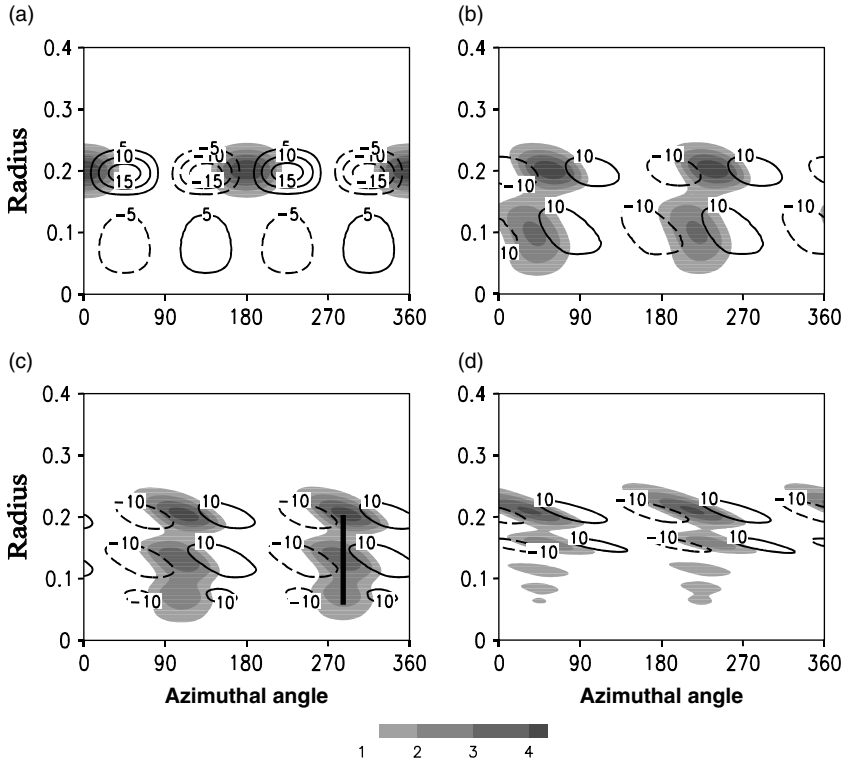

Figure 5. The total vorticity tendency (unit 2.5×10^{-9} s^{-2}) at time (a) 0.0, (b) 0.54, (c) 1.08 and (d) 2.16 for LT020 (initial asymmetric maximum at twice the RMW). Shading represents the positive asymmetric vorticity (unit 5×10^{-5} s^{-1}). An increasing tangential angle is downstream for the basic cyclonic flows. The basic angular velocity decreases with the radius (Figure 1(b)) and the solid line in (c) indicates the phase line of the asymmetry.

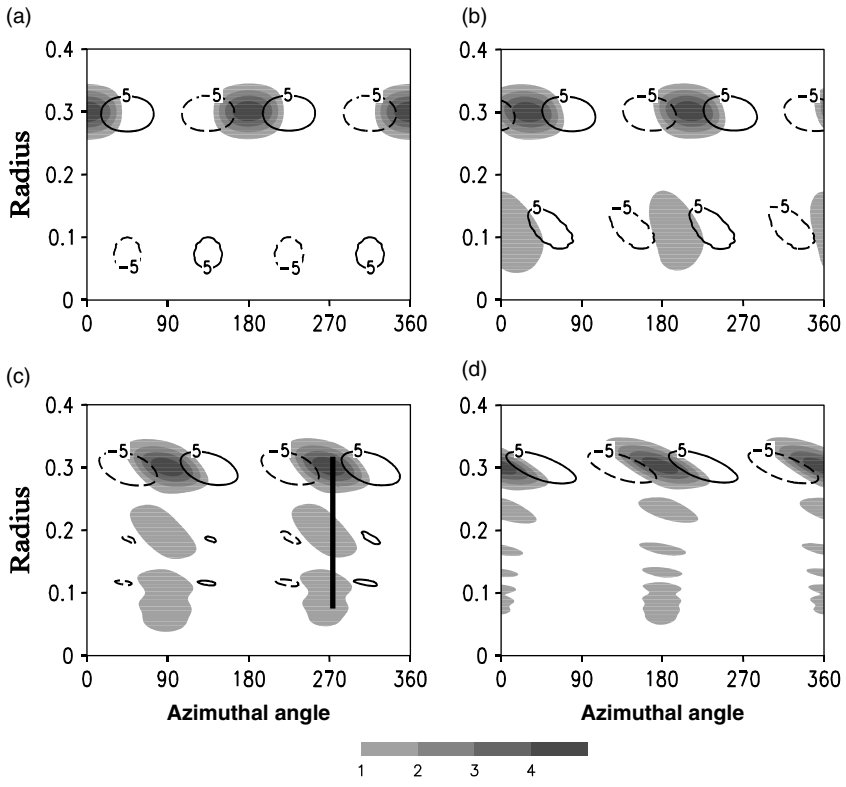

Figure 6. The total vorticity tendency (unit 2.5×10^{-9} s^{-2}) at time (a) 0.0, (b) 0.54, (c) 1.62 and (d) 3.24 for case LT030 (initial asymmetric maximum at three times the RMW). Shading represents the positive asymmetric vorticity (unit 5×10^{-5} s^{-1}). An increasing azimuthal angle is downstream for the basic cyclonic flows. The basic angular velocity decreases with the radius (Figure 1(b)) and the solid line in (c) indicates the phase line of the asymmetry.

DOI: 10.1002/qj

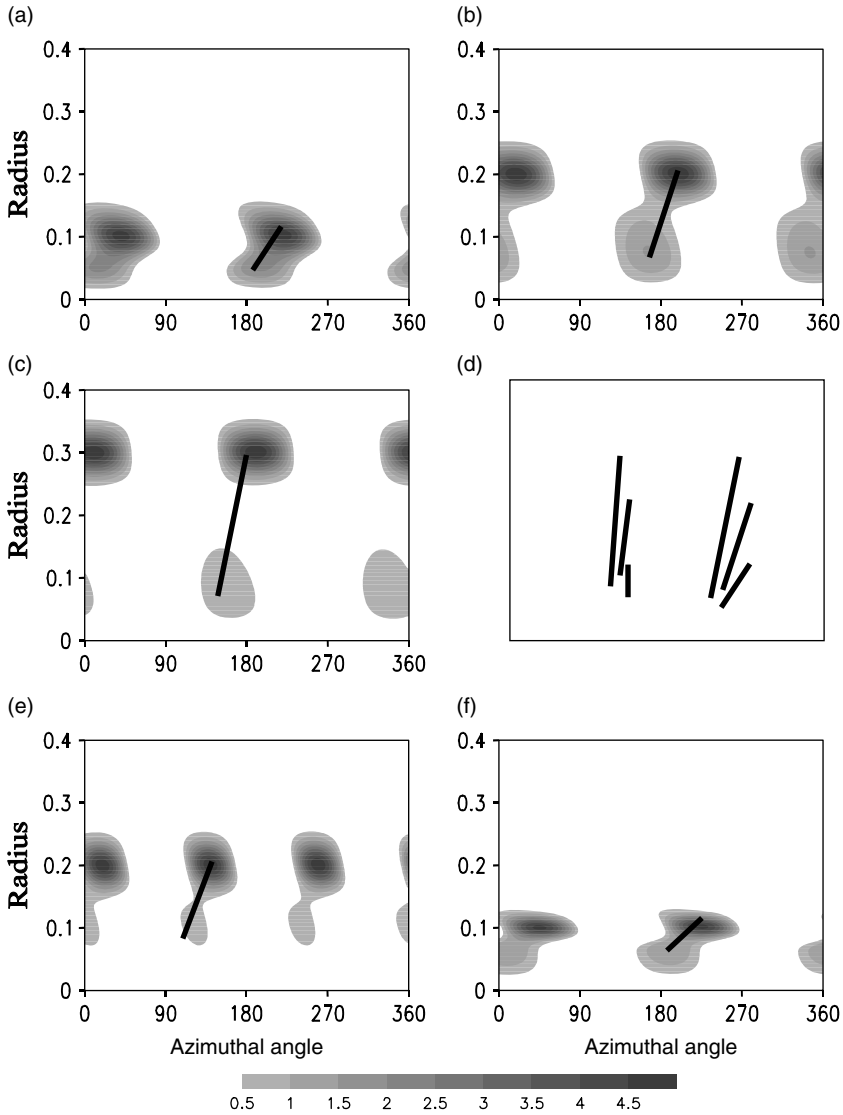

Figure 7. The positive asymmetric vorticity (shading) and phase lines (solid lines connecting the inner and outer asymmetries) at time 0.18 for the cases (a) LT010, (b) LT020, (c) LT030, (e) LU020 and (f) LB010. (d) shows a schematic diagram of the phase lines for cases LT010, LT020 and LT030 at time 0.18 (the three lines on the right) and at time 0.54 (three lines on the left). An increasing azimuthal angle is downstream for the basic cyclonic flows.

the initial asymmetry is placed, the smaller the angle of the upshear phase tilt in the early stage. However, the further the initial asymmetry, the longer time it takes for the differential rotation to change the phase tilt. This differential rotational effect does not occur immediately but develops progressively as the multi-cell asymmetry moves outward. Comparing with the phase lines at time 0.18, the phase angles are smaller at time 0.54 for all three cases (Figure 7(d)). More importantly, the lengths of the phase lines are also shorter than at time 0.18. This results from the fact that the asymmetries at smaller radii propagate outward faster than the asymmetries at greater radii. Therefore, while the inner new asymmetries move outward, there is little outward propagation of the initial asymmetry if it is placed at outer radii. This can be seen in Figures 4, 5 and 6 at different times. The WKB solution by MK97 (their Equation 17), given here as (3.2), shows how the radial group velocity of vortex Rossby waves depends on the local basic-state vorticity gradient

$$C_{\mathrm{gr}} = \frac{-2kn\overline{\zeta}_0'}{R(k^2 + n^2/R^2)^2}, \tag{3.2}$$

where k is the radial wavenumber, n the azimuthal wavenumber, R the local radius and $\overline{\zeta}_0'$ the basic-state vorticity gradient. Thus, according to (3.2) and referring to Figure 1, the radial propagation decreases sharply with increasing radius for a hurricane-like vortex. It is the propagation of the disturbance as a vortex Rossby wave that amplifies the effect of differential rotation when the initial asymmetry is placed at different locations.

In summary, when an asymmetry is placed more outward, its upshear tilt is smaller but the differential

DOI: 10.1002/qj

rotation effect to shift the phase tilt is also smaller. This two effects act against each other in determining how much (and for how long) energy can be transferred from the basic state to the asymmetry. The remaining question is: Is there an optimal radius where the asymmetry placed initially would have the largest energy transfer from the symmetric vortex to the asymmetric perturbations? To answer this question, we engage addition cases with the initial position of the asymmetry placed at $R_p = 0.11$, 0.12, 0.13, 0.14, 0.15, 0.16, 0.17, 0.18, 0.19, 0.22, 0.24, 0.25, 0.26, and 0.28 (Table I).

While the basic state does not change in a linear model, we use the right-hand side of

$$\frac{\partial \overline{v}}{\partial t} = -\overline{u'\zeta'} \tag{3.3}$$

as a proxy to represent the momentum/energy transfer between the symmetric part and the asymmetric perturbation that will be realized in nonlinear simulations. For all the cases from LT010 to LT030 listed in Table I, careful examination of the time evolution of (3.3) indicates that maximum energy transfer occurs when the initial asymmetry is placed around 0.18. The evolution of the tangential wind tendency in LT015, LT018 and LT025 are displayed in Figure 8 for illustration. Negative indicates that the mean tangential wind is weakening and positive indicates the mean wind would increase in a nonlinear simulation. In all cases, there are multiple channels where energy 'can be' transferred between the symmetric and asymmetric components. The further away the initial asymmetry is placed, the more channels there are. In each diagram, the positive energy transfer (i.e. the basic state is gaining) is located near and always slightly inward of the initial asymmetry maximum. New asymmetry is induced inside the initial asymmetry in the early stage but it weakens later as indicated by the negative regions. The LT018 represents the case where the asymmetric perturbations have the largest energy gain from the symmetric vortex near the RMW (Figure 8(b)). Asymmetries are also induced outward of the initial asymmetry. This is consistent with diagnostics for LT010, LT020 and LT030.

To depict more clearly an optimal radius, where the largest energy transfer from the symmetric vortex to the asymmetric perturbations occurs, the minimum (i.e. energy goes to the asymmetry) values near RMW are plotted in Figure 9 as a function of the initial positions of the asymmetry for all the LT series (with the broad profile and wavenumber-two structure). The maximum decrease of the symmetric wind occurs when the initial asymmetry is placed around 0.18. To validate the results above, we also calculate the energy transfer from the symmetric vortex to the asymmetric perturbations near RMW, and use it to identify the optimal radius. The result is similar.

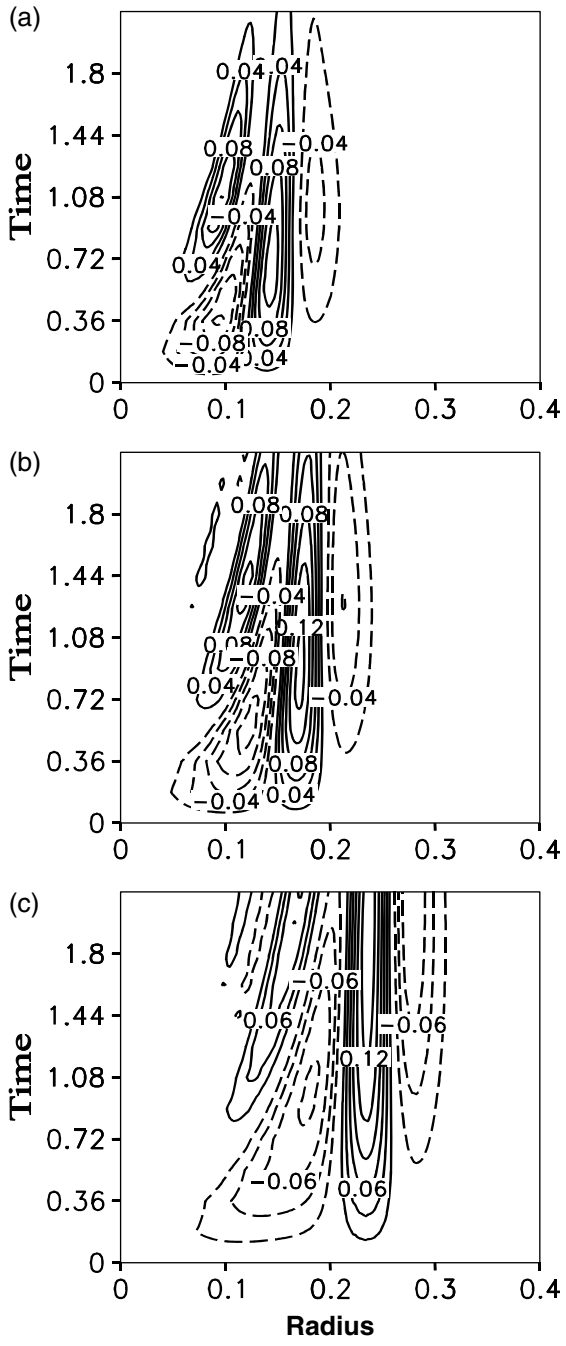

Figure 8. The evolution of the tangential wind tendency (unit 2.5×10^{-3} m s^{-2}) in cases (a) LT015, (b) LT018 and (c) LT025. The unit of radius is 1000 km and time 0.18 = 1 hour.

3.2. Initial asymmetries with the broad profile and a wavenumber-three structure

We further examine the effect of different azimuthal wavenumbers on the axisymmetrization. Cases LU010, LU012 ($R_p = 0.10$, 0.12) etc., have the same initial asymmetry profile as in LT010 (Figure 2, solid line) but with wavenumber-three perturbation (Table I).

The time evolution of the asymmetric KE for the cases LU010, LU020 and LU030 are shown in Figure 10(a–c). Comparing to cases with wavenumber-two asymmetries (Figure 3(d–f)), the wavenumber-three asymmetries generate much weaker asymmetry inside the initial disturbances. Note that the phase tilt comes from the downstream shift of the vorticity advection by basic

DOI: 10.1002/qj

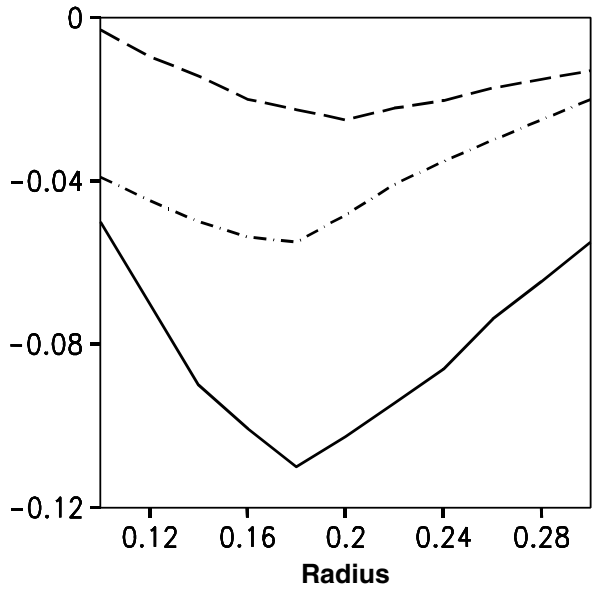

Figure 9. The minimum of tangential wind tendency as functions of the initial positions of the perturbations with the broad profile and wavenumber-two structure (solid line), the broad profile and wavenumber-three structure (dashed line) and the narrow profile and wavenumber two structure (dash-dot line).

symmetric tangential wind (Figure 4(a)) and the upstream shift of the vorticity change by the radial asymmetric wind (Figure 4(b)). As the azimuthal wavenumber increases, the azimuthal wavelength of the asymmetry decreases and these stream-wise shifts become smaller and the upshear tilt becomes smaller (Figure 7(e)). The maximum tangential wind tendency is only about 25% of the wavenumber-two asymmetries. Therefore, the larger the wavenumber, the smaller the growth of the new asymmetry and the quicker the asymmetry will start weakening. This is consistent with earlier studies, such as Carr and Williams (1989), but explained from a different perspective.

Similarly, there exists an optimal radius at $R_p = 0.20$ where the tangential wind tendency is the minimum (Figure 9) for the wavenumber-three asymmetry. The dependence of the energy transfer on the position of the initial asymmetry is similar to the wavenumber-two asymmetry.

3.3. Initial asymmetries with the narrow profile and a wavenumber-two structure

Cases with the narrow asymmetric radial profile are investigated with an azimuthal wavenumber-two structure only (Figure 2, long-short dashed line for LB010). With this narrow profile, the asymmetry can be placed at smaller radii including $R_p = 0.05$, 0.06, 0.07, 0.08, 0.09, 0.10, 0.12, 0.14, 0.16, 0.18, 0.20, 0.22, 0.24, 0.26, 0.28, and 0.30 (Table I). The asymmetric KE evolution for the three major cases LB010, LB020 and LB030 are given in Figure 10(d–f). In comparison to cases with the broad profile (Figure 3), the temporal patterns are similar except that the process for the generation of the inner asymmetry is slower so that the total axisymmetrization will take longer to complete. This is attributed to a larger phase tilt as the radial scale of the initial asymmetry decreases (Figure 7(f)). When the asymmetry is placed at the RMW, the inner new asymmetry is slightly greater than its counterpart with the broad asymmetry profile. When the initial asymmetry is placed at a greater distance, weaker asymmetric winds induce a weaker new asymmetry and the axisymmetrization is very slow.

For this category, the maximum symmetric wind tendency occurs when the initial asymmetry is placed near $R_p = 0.18$ (the optimal radius, Figure 9). Overall, these patterns are similar for the three different categories we investigated (Figure 9).

The initial amplitude of the asymmetry specified is 25% of the basic-state vorticity. One reason for this choice is to compare our results with MK97. Another reason for choosing a large asymmetry is to make the axisymmetrization effect more discernable in the nonlinear simulations. A relatively small asymmetry is used to check the validity of our conclusion from the linear simulation. Experiments are repeated with the initial asymmetric amplitude reduced by half (i.e. 12.5% of the basic-state vorticity). The results are nearly the same regarding the time evolution pattern and the location of the optimal radius. Further reduction of the asymmetric amplitude to less than 10% of the symmetric vorticity also shows similar results.

Another issue is the formulation of the initial asymmetry for experiments with different initial positions. Since the initial asymmetry is specified by equal vorticity, the same maximum vorticity placed at different positions would have different KE. Comparing the initial amplitudes of the three cases in Figure 3 shows that, with the same vorticity profile, asymmetries located at outer radii have larger KE. While it is difficult to specify the same initial KE at different locations for the nondivergent barotropic model, the effect of different KE at different initial locations can be examined by comparing a case located at an inner radius to a case at an outer radius with reduced vorticity so that the maximum KE is roughly the same. Our conclusion regarding the effect of different positions does not change with this consideration.

4. Nonlinear axisymmetrization

While the linear experiments illustrated above show how asymmetries with different characteristics evolve, they do not contain the feedback of the perturbation energy change to the symmetric basic flow. A complete picture of the axisymmetrization can only be obtained in the nonlinear model (A.1) that allows full wave–mean flow interactions. This will be examined in the nonlinear simulations (NT010, NT020 and NT030) with the same initial conditions as in the linear cases LT010, LT020 and LT030. The effect of wave–mean flow interactions can

DOI: 10.1002/qj

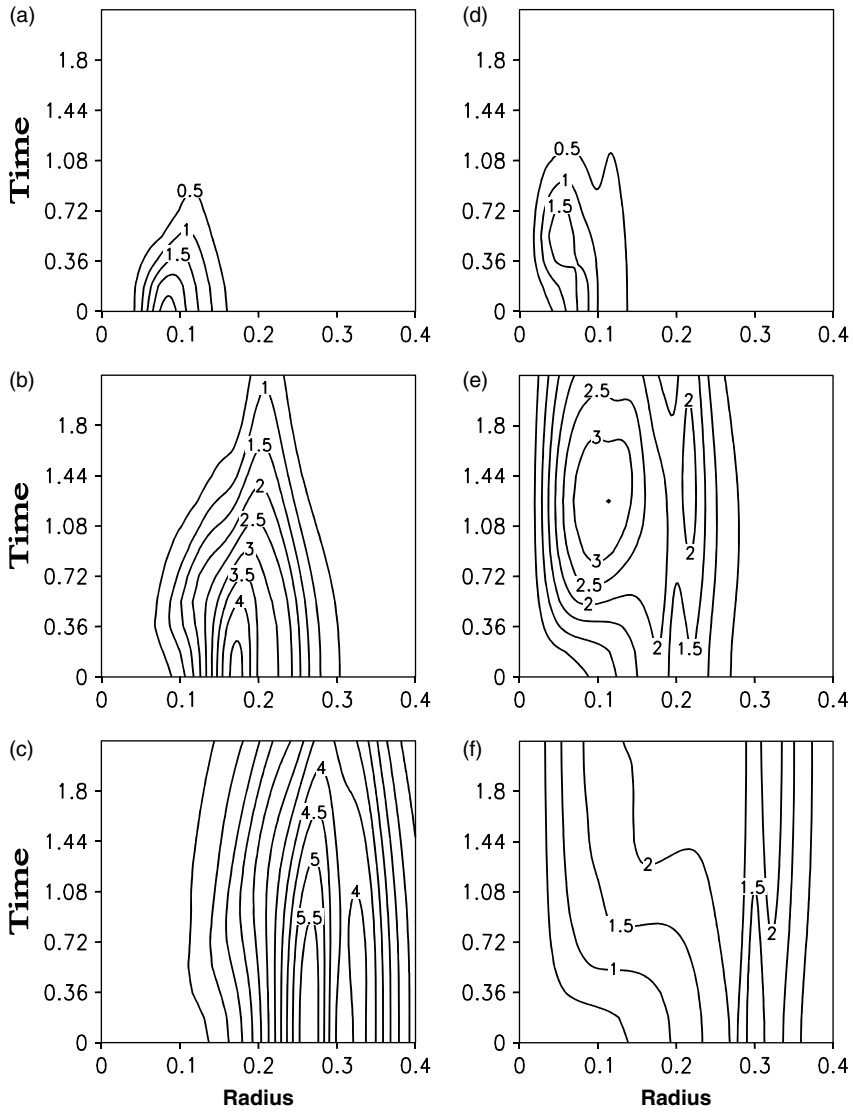

Figure 10. The time–radius cross-section of the asymmetric kinetic energy (unit 2.5×10^3 m^2 s^{-2}) in the linear case (a) LU010, (b) LU020, (c) LU030 for the initial wide profile and wavenumber-three perturbations, and (d) LB010, (e) LB020 and (f) LB030 for the initial narrow profile and tangential wavenumber-two perturbations.

be discerned from the symmetric KE equation:

$$\frac{\partial \overline{K}}{\partial t} = -\frac{\partial (r\overline{u}\,\overline{K})}{r\partial r} - \overline{u}\frac{\partial (r\overline{u'^2})}{r\partial r} - \overline{v}\frac{\partial (\overline{u'v'})}{\partial r} + \overline{u}\frac{\overline{v'^2}}{r} - \frac{2\overline{v}}{r}\overline{u'v'} - \overline{u}\frac{\partial \overline{\varphi}}{\partial r}, \qquad (4.1)$$

where the first term on the right-hand side is the flux divergence of $\overline{K}$ by symmetric radial flow, the sum of the second, third, fourth and fifth term represents the symmetric KE change by wave–wave interactions, and the sixth term is the energy conversion of symmetric potential energy into symmetric KE. The first and the last term on the right-hand side do not involve the disturbance and are not related to energy transfer between the asymmetry and the symmetry.

In the nonlinear experiment NT010, the asymmetry generated inside the initial maximum disturbance is weaker than in the linear experiment LT010 (Figures 11(a, b) versus 3(a, d)). The outward propagation of the asymmetric KE is also more confined (Figure 11(b)). The symmetric tangential wind (Figure 11(c)) grows at the expense of the weakening of the asymmetry before time 1.62, also shown by the KE exchange between them (Figure 11(d)). The maximum increment of the symmetric tangential wind is located at the radius of 0.09 just inside the RMW and very close to the location of the initial asymmetry. Outside the region of the initial asymmetry maximum (between the radius of 0.14 and 0.2), an energy transfer from the symmetric to the asymmetric part (Figure 11(d)) occurs as the asymmetry propagates outward (Figure 11(b)). The tangential wind at time 2.16 for this case is shown later, along with other cases.

The second and the fourth term on the right-hand side of (4.1) are at least two orders of magnitude smaller than the third and fifth term, so only the latter two terms are

DOI: 10.1002/qj

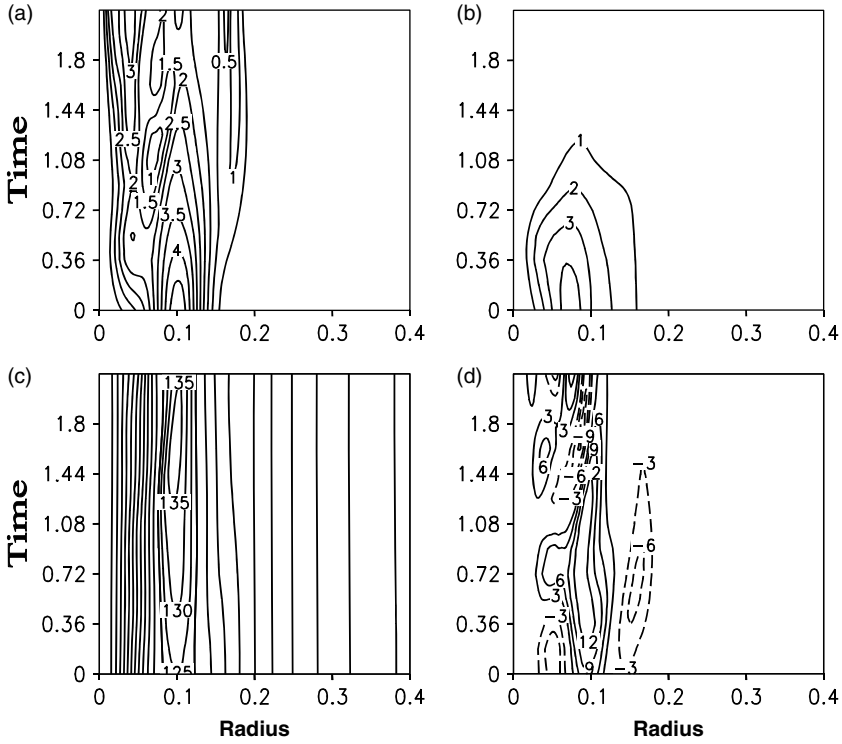

Figure 11. The time–radius cross-section of (a) the asymmetric vorticity amplitude, (b) the asymmetric KE, (c) the symmetric KE and (d) the symmetric KE change rate by wave–wave interactions in the nonlinear case NT010 with the initial broad radial profile and wavenumber-two perturbations.

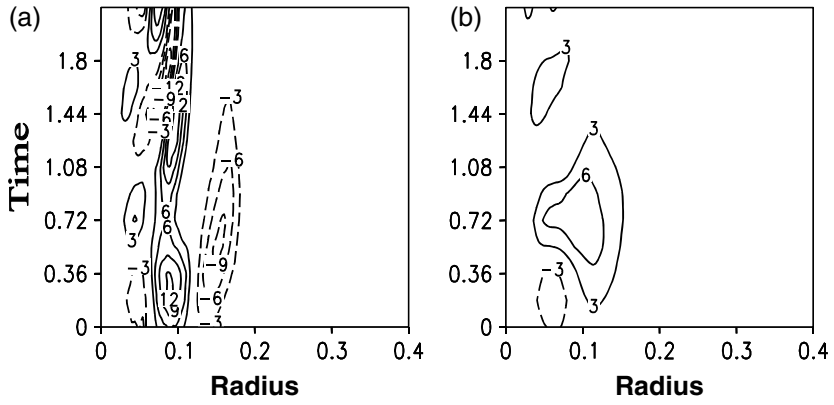

Figure 12. Two components of the symmetric KE change rate by wave–wave interactions in the nonlinear case NT010: (a) $-\overline{v}\partial(\overline{u'v'})/\partial r$, and (b) $-2(\overline{v}/r)\overline{u'v'}$.

shown in Figure 12. Comparing Figures 12 and 11(d), the generation of the symmetric energy near the RMW is through the fifth term due to the downshear tilt of the disturbance ($-\overline{u'v'} > 0$, Figure 12(b)) as well as the third term as $-\overline{u'v'}$ increases with r (Figure 12(a)). The symmetric part loses its energy to the asymmetry near the radius 0.15 because the eddy momentum flux ($-\overline{u'v'}$) decreases with r(the third term). This is similar to the upscale energy transfer from synoptic waves to zonal mean flows for upper-level midlatitude jets.

For the NT020 case (Figure 13(a)), only a weak asymmetry is generated near RMW, in contrast to the multiple asymmetries in the linear case (LT020, Figure 3(b)). This may be due, in part, to the fact that the symmetric part has been modified in the nonlinear case. In addition, the initial asymmetry propagates inward (outward) in the nonlinear (linear) case. The energy exchange (Figure 13(c)) shows a loss of energy from the basic state to the disturbance (near the RMW), resulting in a weakening of the symmetric flow before time 0.72 (Figure 13(b)) and a gain of energy from the disturbance between time 0.72 and 1.62. The symmetric part losses its energy to the asymmetry again after time 1.62. Diagnostics using (4.1) indicate that the energy exchange is also dominated by the eddy momentum flux and the gradient of it as in the NT010 (not shown). As the basic state continues

DOI: 10.1002/qj

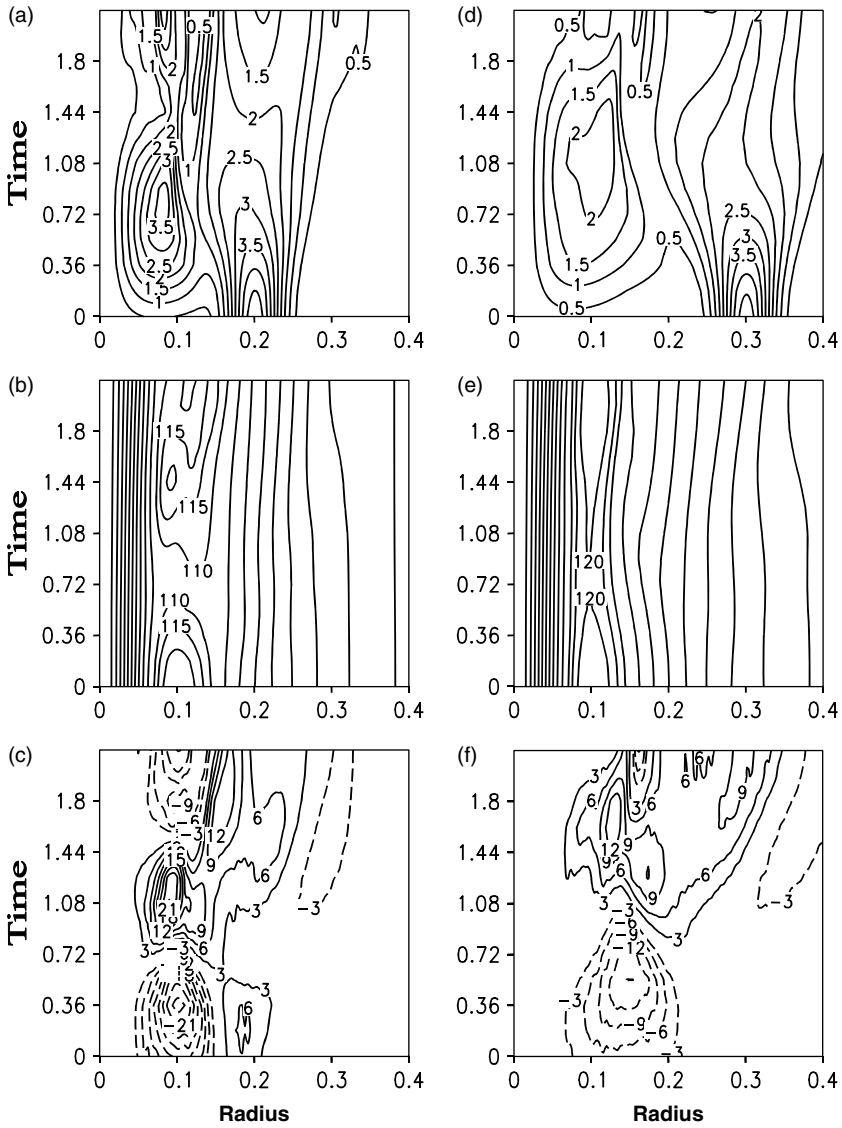

Figure 13. The time evolution of (a, d) the asymmetric vorticity amplitude, (b, e) the symmetric KE and (c, f) the symmetric KE change rate by wave–wave interactions in the nonlinear cases (a–c) NT020 and (d–f) NT030.

gaining energy in the outer region ($r = 0.15 \sim 0.2$), a double-peak structure appears in the tangential wind at time 2.16 (Figure 14(c)).

When the initial disturbance in NT030 is placed far away from the area with large basic-state vorticity gradient, the KE exchange rate by the wave–wave interactions is smaller than that in NT020 (Figure 13(f) versus 13(c)), leading to a weaker asymmetry inside the initial perturbation (Figure 13(d)) and less change in the symmetric wind (Figure 13(e)). The asymmetry sustains its energy longer and the axisymmetrization takes longer to complete. The symmetric wind loses its energy near the RMW in the early stage but gains the energy back at a later stage. This is what we expect based on the linear case.

Another two nonlinear cases, NT015 and NT025, are included to provide a more complete picture on how the position of the initial asymmetry affects the outcome of the basic state through axisymmetrization. The rate of change of the symmetric KE due to the wave–wave interactions and the evolution of the maximum tangential winds at the RMW for the five cases are shown in Figure 14. In the NT010 case, the basic state gains energy from the asymmetric part until time 1.62 (Figure 14(a, b)). For the four remaining cases, energy is being transferred from the symmetric component to the asymmetry in the early stage, followed by a period of energy transfer from the asymmetry back to the symmetric component. This process is oscillatory, typical with nonlinear interactions. Among the five cases shown, case NT020 has the largest fluctuation of energy transfer as its initial asymmetry is placed near the optimal radius, as discussed earlier.

The tangential wind profiles at time 2.16, when the axisymmetrization process has nearly completed, are depicted in Figure 14(c). Case NT010 gives the largest increase of the maximum tangential wind, followed by NT015. NT015 has its RMW moved slightly outward as a result of energy redistribution during the

DOI: 10.1002/qj

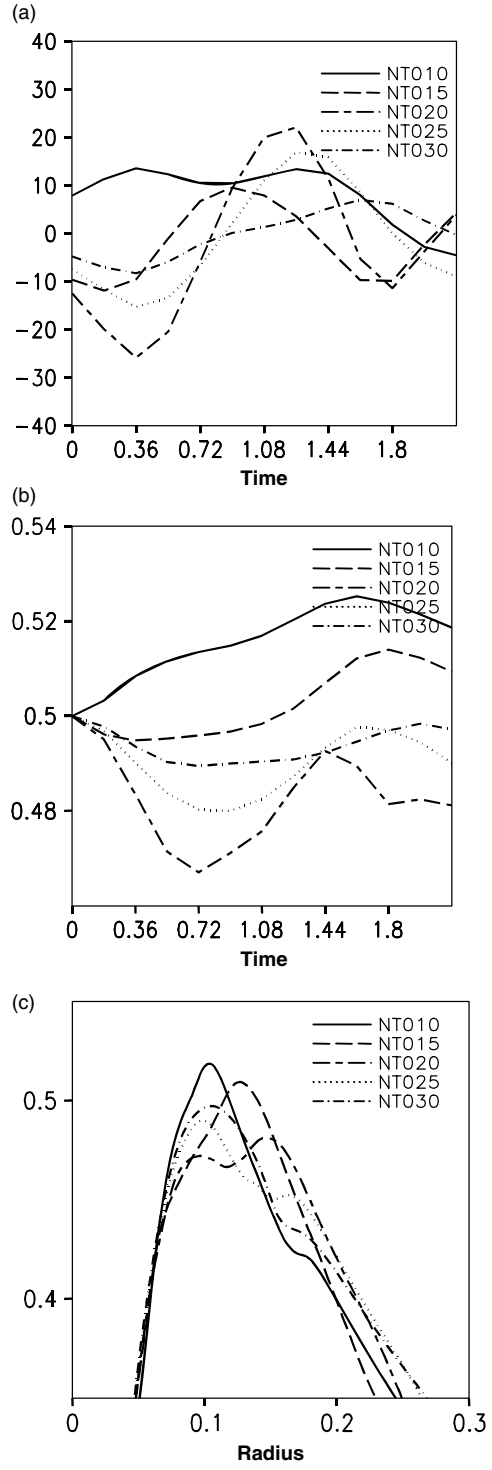

Figure 14. (a) Evolution of symmetric KE change rates by wave–wave interactions at the RMW; (b) temporal change of the maximum tangential wind; (c) tangential wind profiles at time 2.16 in nonlinear cases NT010, NT015, NT020, NT025 and NT030 for the initial broad profile wavenumber-two asymmetry.

axisymmetrization. NT020 has a wider wind band with two maxima. The two cases in which the asymmetries are placed further out see their symmetric wind speed increase in the outer part. These results indicate that, in order to increase the maximum intensity of a tropical cyclone through axisymmetrization of asymmetries, the asymmetries have to be located near the RMW. For asymmetries imposed at a greater radius, the axisymmetrization process can increase the symmetric wind in the outer part, or even create double peaks. This is the effect of the growth of inner asymmetries and differential propagations of the asymmetries as vortex Rossby waves.

5. Summary and discussion

In this study, linear and nonlinear non-divergent barotropic models are used to investigate how asymmetric disturbances, generated by external forces, can have different effects on vortex axisymmetrization. The linear experiments show that an initially imposed asymmetry would generate a new asymmetry inside the original asymmetry at the radius where the basic-state vorticity gradient is largest. The phase tilt of the asymmetry is upshear in the early stage so that the asymmetry gains energy from the basic state. Differential rotation of the basic state then shifts the phase of the asymmetry to a downshear tilt and the asymmetry weakens. The further out the initial asymmetry is, the smaller is the initial upshear tilt. However, the further out the initial asymmetry is, the smaller is the differential rotation effect so that the asymmetry can sustain its upshear tilt longer. These two competing mechanisms act against each other and determine how large and how long the energy transfer is between the basic state and the asymmetry. An optimal radius, where an asymmetry placed initially would have the largest energy transfer between itself and the symmetric part, can be determined. This is illustrated schematically in Figure 15 by the three experiments where the initial asymmetry is placed at the RMW, twice the RMW and three times the RMW, respectively. From more experiments with small incremental radial distance of the initial asymmetry, the optimal radius is found to be about 1.8 times the RMW for our given profile. The larger the azimuthal wavenumber, the smaller is the initial upshear tilt, due to smaller azimuthal wavelength. Thus an asymmetry with larger wavenumber can be sheared

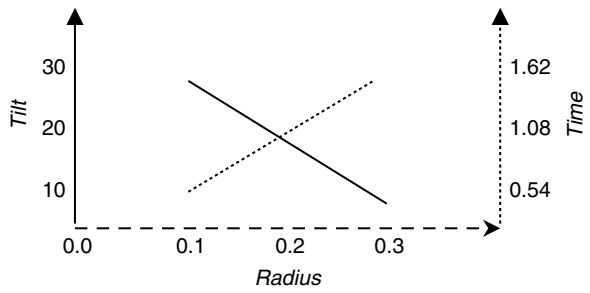

Figure 15. Schematic diagram illustrating the optimal radius based on the cases LT010, LT020 and LT030. The horizontal axis indicates the radial position where the initial disturbance is placed. The left vertical axis displays the angle (degrees) of initial upshear tilt. The right vertical axis is the time when the upshear tilt changes to neutral.

DOI: 10.1002/qj

quicker by the basic state, losing its energy to the basic state faster. For the same basic-state profile, there is little change of the optimal radius with a different azimuthal wavenumber or a narrower asymmetric radial profile.

The concept of optimal radius is further examined for its generality with five different basic-state profiles (not shown), representing wind profiles for different speed and sizes of hurricane-like vortices. An optimal radius can be found for each individual profile and their values fall between 1.5 to 2.0 times the RMW.

The WKB solution for the dispersion relation of the vortex Rossby waves from MK97 is used to explain different propagation speeds of an asymmetry at different locations. This differential propagation plays an important role in determining the differential rotation effect in that an asymmetry placed initially at a greater distance has a smaller differential rotation effect so that the asymmetry can maintain an upshear tilt longer. There are multiple channels of outward energy propagation in the linear simulations inside the initial asymmetry.

When nonlinear effects are included, the general characteristics of the evolution of the asymmetry are similar to the linear solutions. However, in the nonlinear simulations, the new inner asymmetry is weaker and the multi-channel outward propagations of the asymmetries are less obvious and more confined. When an asymmetry is placed near the RMW initially, the asymmetry loses energy to the basic state quickly after a brief period of energy gain so that the symmetric vortex has a larger maximum wind (intensity). When the initial asymmetry is placed further out from the core, the basic-state vortex loses energy to the newly generated asymmetry in the early stage and then gains the energy back as the asymmetry tilts downshear and propagates outward slowly. If the new inner asymmetry grows more intense, the restoration of the basic-state energy may not be back to the same radius where the initial energy loss occurred, due to the radial propagation of the asymmetry. The final state of the symmetric vortex may have a smaller maximum intensity but larger size (an increase of wind in the outer part), or even a double-peak profile, after the axisymmetrization process is completed. The maximum intensity of the vortex increases only when the initial asymmetry is imposed near the RMW. Overall, deposition of the asymmetric energy on the symmetric part is most pronounced near the radius at which the asymmetry is initially imposed. This, of course, also depends on the radial profile of the asymmetry. If a fairly localized asymmetry is imposed far away from the core, it would have very little impact on the maximum intensity of the symmetric flows through axisymmetrization.

Nolan and Grasso (2003) considered both thermal and velocity disturbances and found the final near-steady-state results similar. When a velocity forcing is placed at twice the distance of the radius of the maximum wind, the weakening of the symmetric wind is not as dramatic as a thermal disturbance placed at the same place. The maximum change of the velocity, after the major process has completed, is near the location where the asymmetry is initially placed. Our results are consistent with theirs in this aspect.

While some of the characteristics of the axisymmetrization were observed in early studies (i.e. MK97; MM99; Nolan and Grasso, 2003), this study highlights the impacts that asymmetries at different locations may have on the hurricane intensity and size change. In addition, we propose an important, practically useful concept for the existence of an optimal radius at which an initial asymmetric perturbation may have the largest energy gain from the symmetric vortex. In MM99, the impact of the asymmetry on the basic-state vortex is about 2% of the maximum tangential velocity even when their initial asymmetric vorticity is 40% of the basic-state vorticity. In our nonlinear simulations, the modification of the basic-state velocity is between 5 to 10% with our initial asymmetry being 25% of the symmetric part. The change to the symmetric wind may appear to be small. It represents, however, only the impact of a single disturbance. In reality, asymmetric disturbances are being generated all the time and the cumulative axisymmetrization effect can be substantial.

Acknowledgements

This work was supported by ONR grants N000140710145, N000140810256, PE 0602435N and NRL subcontract N00173-06-1-G031, and National Natural Science Foundation of China under Grants 40205009 and 40333025. The International Pacific Research Center is partially sponsored by the Japan Agency for Marine-Earth Science and Technology (JAMSTEC), NASA (NNX07AG53G) and NOAA (NA17RJ1230). This is SOEST publication number 7481 and IPRC publication number 530.

Appendix

This appendix delineates the nonlinear and linear barotropic models in non-dimensional form on a constant-f plane.

A.1 Nonlinear barotropic model

$$\frac{\partial u}{\partial t} + u\frac{\partial u}{\partial x} + v\frac{\partial u}{\partial y} - v = -\frac{\partial \phi}{\partial x}, \tag{A.1a}$$

$$\frac{\partial v}{\partial t} + u\frac{\partial v}{\partial x} + v\frac{\partial v}{\partial y} + u = -\frac{\partial \phi}{\partial y}, \tag{A.1b}$$

$$-2J(u, v) - \zeta = -\nabla^2\phi, \tag{A.1c}$$

where $J(u, v) = \frac{\partial u}{\partial x}\frac{\partial v}{\partial y} - \frac{\partial v}{\partial x}\frac{\partial u}{\partial y}$ and $\zeta = \frac{\partial v}{\partial x} - \frac{\partial u}{\partial y}$.

A.2 Linear barotropic model

$$\frac{\partial u'}{\partial t} + \overline{u}\frac{\partial u'}{\partial x} + \overline{v}\frac{\partial u'}{\partial y} + u'\frac{\partial \overline{u}}{\partial x} + v'\frac{\partial \overline{u}}{\partial y} - v' = -\frac{\partial \varphi'}{\partial x}, \tag{A.2a}$$

DOI: 10.1002/qj

$$\frac{\partial v'}{\partial t} + \overline{u}\frac{\partial v'}{\partial x} + \overline{v}\frac{\partial v'}{\partial y} + u'\frac{\partial \overline{v}}{\partial x} + v'\frac{\partial \overline{v}}{\partial y} + u' = -\frac{\partial \varphi'}{\partial y}, \tag{A.2b}$$

$$\frac{\partial}{\partial x}\left(\overline{u}\frac{\partial u'}{\partial x} + \overline{v}\frac{\partial u'}{\partial y} + u'\frac{\partial \overline{u}}{\partial x} + v'\frac{\partial \overline{u}}{\partial y}\right) + \frac{\partial}{\partial y}\left(\overline{u}\frac{\partial v'}{\partial x} + \overline{v}\frac{\partial v'}{\partial y} + u'\frac{\partial \overline{v}}{\partial x} + v'\frac{\partial \overline{v}}{\partial y}\right) - \zeta' = -\nabla^2\varphi', \tag{A.2c}$$

where u and v are the horizontal wind velocity components, ϕ is the geopotential height, and ζ the vorticity. Variables with an overbar represent the basic states and those with a prime are the perturbations, otherwise they represent the total field.

References

Carr LE III, Williams RT. 1989. Barotropic vortex stability to perturbations from axisymmetry. *J. Atmos. Sci.* **46**: 3177–3191.

Case KM. 1960. Stability of inviscid plane Couette flow. *Phys. Fluids* **3**: 143–148.

Enagonio J, Montgomery MT. 2001. Tropical cyclogenesis via convectively forced vortex Rossby waves in a shallow-water primitive equation model. *J. Atmos. Sci.* **58**: 685–705.

Guinn TA, Schubert WH. 1993. Hurricane spiral bands. *J. Atmos. Sci.* **50**: 3380–3403.

MacDonald NJ. 1968. The evidence for the existence of Rossby-like waves in the hurricane vortex. *Tellus* **20**: 138–150.

McCalpin JD. 1987. On the adjustment of azimuthally perturbed vortices. *J. Geophys. Res.* **92**: 8213–8225.

Melander MV, McWilliams JC, Zabusky NJ. 1987. Axisymmetrization and vorticity-gradient intensification of an isolated two-dimensional vortex through filamentation. *J. Fluid Mech.* **178**: 137–159.

Möller JD, Montgomery MT. 1999. Vortex Rossby-waves and their influence on hurricane intensification in a barotropic model. *J. Atmos. Sci.* **56**: 1674–1687.

Möller JD, Montgomery MT. 2000. Tropical cyclone evolution via potential vorticity anomalies in a three-dimensional balance model. *J. Atmos. Sci.* **57**: 3366–3387.

Möller JD, Shapiro LJ. 2005. Influence of asymmetric heating on hurricane evolution in the MM5. *J. Atmos. Sci.* **62**: 3974–3992.

Montgomery MT, Enagonio J. 1998. Tropical cyclogenesis via convectively forced vortex Rossby waves in a three-dimensional quasigeostrophic model. *J. Atmos. Sci.* **55**: 3176–3207.

Montgomery MT, Kallenbach RJ. 1997. A theory for vortex Rossby-waves and its application to spiral bands and intensity changes in hurricanes. *Q. J. R. Meteorol. Soc.* **123**: 435–465.

Nolan DS, Farrell BF. 1999a. Generalized stability analyses of asymmetric disturbances in one- and two-celled vortices maintained by radial inflow. *J. Atmos. Sci.* **56**: 1282–1307.

Nolan DS, Farrell BF. 1999b. The intensification of two-dimensional swirling flows by stochastic asymmetric forcing. *J. Atmos. Sci.* **56**: 3937–3962.

Nolan DS, Grasso LD. 2003. Nonhydrostatic, three-dimentional perturbations to balanced, hurricane-like vortices. Part 2: Symmetric response and nonlinear simulations. *J. Atmos. Sci.* **60**: 2717–2745.

Nolan DS, Montgomery MT. 2002. Nonhydrostatic, three-dimentional perturbations to balanced, hurricane-like vortices. Part 1: Linearized formulation, stability, and evolution. *J. Atmos. Sci.* **59**: 2989–3020.

Shapiro LJ. 2000. Potential vorticity asymmetries and tropical cyclone evolution in a moist three-layer model. *J. Atmos. Sci.* **57**: 3645–3662.

Shen TL, Tian YX, Ge XZ, Lu WS, Chen DH. 2003. *Numerical weather prediction.* Beijing Meteorology Press: (in Chinese).

Smith GB, Montgomery MT. 1995. Vortex axisymmetrization: Dependence on azimuthal wave-number or asymmetric radial structure changes. *Q. J. R. Meteorol. Soc.* **121**: 1615–1650.

Sutyrin GG. 1989. Azimuthal waves and symmetrization of an intense vortex. *Sov. Phys. Dokl.* **34**: 104–106.

DOI: 10.1002/qj